16th World Conference on Earthquake, 16WCEE 2017
Santiago Chile, January 9th to 13th 2017
Paper N° 2816 (Abstract ID)
Registration Code: S- O1463146180

# STRUCTURAL RESPONSE DUE TO SUPERSHEAR AND SUBSHEAR RUPTURE BASED ON DYNAMIC RUPTURE MODEL

T. Hashimoto[(1)], M. Nagano[(2)], K. Kato[(3)], Y. Ohtsuka[(4)], T. Uetake[(5)], K. Hikima[(6)]

[(1)] *Graduate student, Tokyo University of Science, 7111101@alumni.tus.ac.jp*
[(2)] *Professor, Tokyo University of Science, nagano-m@rs.noda.tus.ac.jp*
[(3)] *Senior General Manager, Kobori Research Complex Inc., katokenichi@kajima.com*
[(4)] *General Manager, Project Management Department, Kobori Research Complex Inc., yohtsuka@kobori-rc.com*
[(5)] *Specialist, Tokyo Electric Power Company Holdings, Inc., uetake.tomiichi@tepco.co.jp*
[(6)] *Specialist, Tokyo Electric Power Company Holdings, Inc., hikima.kazuhito@tepco.co.jp*

## *Abstract*

In estimation of a seismic capacity of a building, it is important to consider various patterns of external forces that can be generated from a rupture of a seismic fault.

Currently, kinematic rupture models assuming fault rupture pattern a priori are widely used for numerical predictions of strong motion. However, some studies have used dynamic rupture models based on the friction laws. It is generally assumed in the kinematic rupture models that a rupture velocity is less than the S-wave velocity in the rupture process, which is called “subshear rupture.” However, in some cases, the rupture velocity is faster than the S-wave velocity, which is called “supershear rupture.” The dynamic rupture model can express supershear rupture as a consequence of spontaneous rupture based on physically consistent models, without arbitrary assumption of rupturing process including spatial velocity and slip time function. From the structural engineer's point of view, it is important to consider the response of buildings to pulse-like waves accompanied by supershear rupture to predict the building damage and to estimate seismic performance in all possible scenarios.

In this paper, we calculate dynamic ruptures by varying parameters, and present a detailed discussion of ground motion characteristics under various parameters, focusing on the slip-weakening law, the fault length, and the depth of the initial crack. The investigated rupture patterns include subshear rupture, supershear rupture, and the transition from subshear rupture to supershear one. In addition, the impact to a building of applying ground motions caused by supershear rupture to a building is discussed.

*Keywords: Supershear rupture, Subshear rupture, Dynamic rupture model, Pulse-like ground motion*

# 1. Introduction

In estimating of a seismic capacity of a building, it is important to consider various patterns of external forces generated from the rupture of seismic faults.

Currently, the general method for evaluating strong ground motion based on theoretical calculations uses the kinematic rupture models, in which size of the seismic fault and rupture velocity, $V_r$, and slip time functions are given as prior information. In contrast, dynamic rupture models can express rupture process of fault plane according to a friction law[1)]. A slip-weakening friction law is generally used for dynamic rupture model. The rupture characteristics of a seismic fault can be defined by the parameters of the slip-weakening friction law, resulting in various types of pulse-like ground motions. In kinematic rupture models, $V_r$, is generally assumed to be subshear, meaning the S-wave velocity, $V_s$, is greater than $V_r$. In contrast, the dynamic rupture model can express supershear rupture, in which $V_r$ is greater than $V_s$[2)].

Seismological observations suggest that the propagation of supershear rupture has occurred in some long strike-slip faults[3), 4)]. The spatial distribution and characteristics of pulse-like seismic ground motions caused by supershear rupture have not yet been sufficiently investigated. Small differences in the friction law and initial stress conditions significantly affect rupture properties and ground motion evaluated by numerical simulations based on the dynamic rupture model. Therefore, it is indispensable to perform a detailed sensitive analyses to grasp dependency of parameters in slip-weakening friction law. Pulse-like ground motions have great impact on structural responses including super high-rise buildings. Therefore, from the structural engineer's point of view, it is important to consider the response of buildings to seismic waves caused by supershear rupture to predict the building damage in all possible scenarios.

This paper presents a detailed discussion of the evaluation of the strong ground motion adjacent to the seismic fault caused by supershear rupture. Parameter analyses of the friction law, depth of initial crack, and fault length are conducted. The spatial variation of ground motion pulses and rupture propagation process of fault are considered in the case of supershear rupture. In addition, the differences in the structural response to seismic waves caused by supershear rupture and subshear one are discussed for a 30-story reinforced concrete building.

# 2. Parameter analysis of slip-weakening friction law

## 2.1 Analysis model and parameters of dynamic rupture model

In the first place, the critical displacement, one of the important characteristics of the friction law, is investigated focusing on variation of the rupture process of the seismic fault and the ground motion close to the seismic fault. Fig. 1 shows a slip-weakening friction law used in this study. The ground motion and rupture process on fault was simulated using the three-dimensional finite difference method[1)]. Various dynamic rupture scenarios on a vertical strike-slip fault with surface rupture were simulated in a homogeneous medium. Fig. 2 and Table 1 show parameters and the initial conditions of the basic model. The dimensions of the simulation model were 60 km × 30 km in the horizontal plane, and 30 km in depth. The length and width of the fault plane were set to 30 and 15 km. In addition, the fault plane was set in the center of the simulation model. The grid interval in space was set to 0.1 km, and the analysis time was 15 s with time interval of 0.01 s. The initial crack was set in the center of the fault plane, and a shear fracture starts in the fault plane. Additional stress was applied to the shear stress to make it equal to the static friction stress in the initial crack. Six cases by incrementally changing the critical displacement of the slip-weakening friction law, as shown in Table 2, were studied to observe transition state from subshear to supershear ruptures.

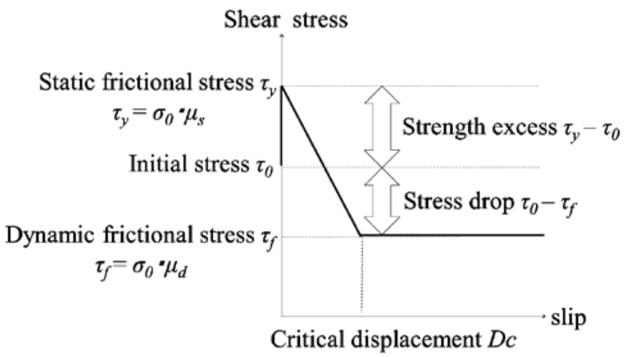


Fig.1 Slip-weakening friction law

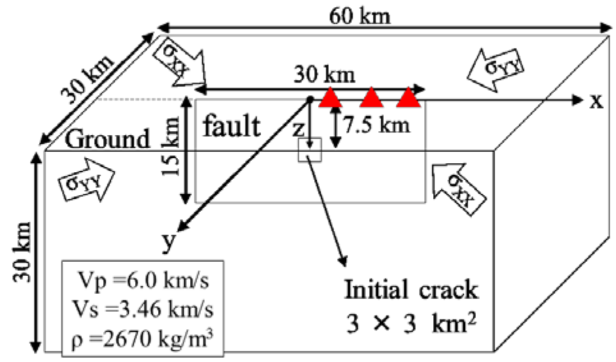


Fig.2 Analysis model

Table 1 Initial conditions of fault in this study

| | |
|---|---|
| Initial stress $\sigma_{xx}$ | –190 MPa |
| Initial stress $\sigma_{yy}$ | –50 MPa |
| Initial stress $\sigma_{zz}$ | 0 MPa |
| Initial shear stress $\tau_0$ | 70 MPa |
| Initail normal stress $\sigma_0$ | –120 MPa |
| Added stress | 11.24 MPa |
| Static coefficient of friction $\mu_s$ | 0.677 |
| Dynamic coefficient of friction $\mu_d$ | 0.525 |
| Critical displacement Dc | 0.4 m |

Table 2 Fault parameters for analysis case

| Critical displacement *Dc* | | |
|---|---|---|
| Name | Meter | Supershear : ✓<br>Subshear : Blank space |
| case1 | 0.40 | |
| case2-1 | 0.18 | |
| case2-2 | 0.16 | |
| case2-3 | 0.14 | ✓ |
| case2-4 | 0.12 | ✓ |
| case2-5 | 0.10 | ✓ |

## 2.2 Effects of critical displacement

Fig. 3 shows contours of the rupture arrival times on the fault for three cases with different critical displacements. In Figs. 3(b) and 3(c), supershear rupture occurred for strike directions in cases with critical displacements of less than 0.14 m. Rupture velocity in the direction of the fault dip also increases when the critical displacement is small, though it does not exceed S-wave velocity. Therefore, the configuration of contours shown in Fig. 3(b) and 3(c) is shaped like a gourd.

Fig.4 shows the maximum ground velocity vectors on the ground surface for the same cases shown in Fig.3. Fig.5 shows the distributions of the maximum velocity, $|V_{max}|$, along the fault on the ground surface. The distribution of $|V_{max}|$ along the *x*-direction is linearly symmetric across the *y*-axis. The magnitude of the velocity in the fault-normal (FN) direction was large around the fault tip in Case 1 under the influence of the rupture directivity effects. However, the velocity vectors was complexed in Cases 2-3 and 2-5, and $|V_{max}|$ peaked behind

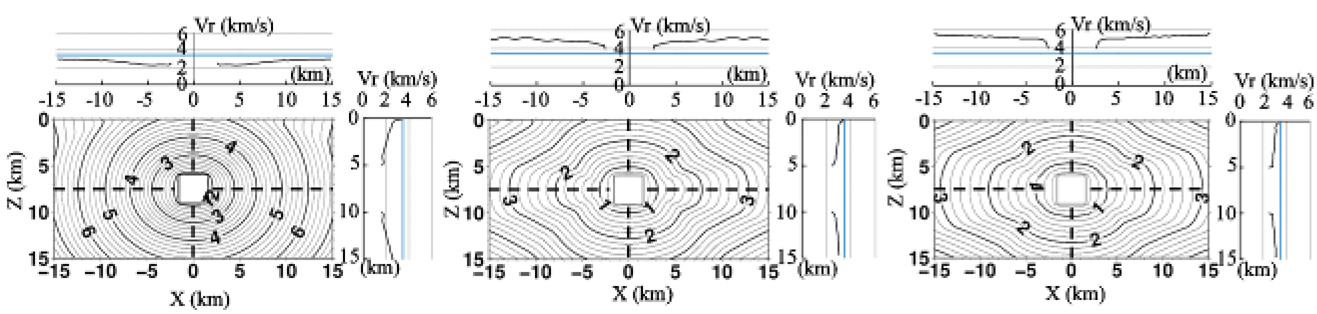


(a) Case 1 (b) Case 2-3 (c) Case 2-5

Fig. 3 Contour plots of rupture front and graphs of the rupture velocity on ground surface the fault tip. The area where the contours of the supershear and subshear regions overlap toward the ground surface from the initial crack is seen as the transition region indicated by thick red lines in Fig.6. Amplification area behind the fault tip corresponds to the transition region, where the difference between $V_r$ and $V_s$ was small and maximum slip velocity of fault is large, as shown in Fig.7[5].

The peak values of $|V_{max}|$ and their locations differed even among the different supershear rupture cases (Fig. 5). The peak value of $|V_{max}|$ in Cases 2-3, 2-4, and 2-5 occurred at $X$ = 10.5, 9.5, and 9.0 km, respectively. The position of the transition region moved from the fault tip to the fault center as the critical displacement decreased (Figs. 6 and 7). Additionally, the peak values of $|V_{max}|$ in Cases 2-3 and 2-5 were 4.35 and 3.48 m/s, respectively. Because the transition region in Case 2-3 was furthest from the fault, the amplitude was increased by the increased rupture directivity effect. Fig. 8 shows the velocity waveforms along the fault on the ground surface. The pulse in Case 1 became large toward the fault tip, but those in Cases 2-3 and 2-5 had two peaks behind the fault tip[4]. One of the plausible reasons for this is due to increases in the difference between $V_r$ and $V_s$. In addition, the velocity waveforms for Case 2-5 showed two peaks closer to the center of the fault than Case 2-3 because the transition region in Case 2-5 was located closer to the fault center than that for Case 2-3 (Figs. 6 and 7).

Fig. 9 shows the pseudo-velocity response spectra pSv (h= 5 %) along the fault on the ground surface. The pSv in Case2-4 and Case2-5 became smaller as the rupture approached the fault tip, but pSv in Case2-3 is largest at the near fault tip. Spatial variation of pSv level for above cases depends on transition region of subshear and supershear rupture. The pSv in the supershear cases was smaller than that in the subshear cases ahead of the fault tip. The predominant periods in the supershear and subshear cases are shorter than 0.5 s.

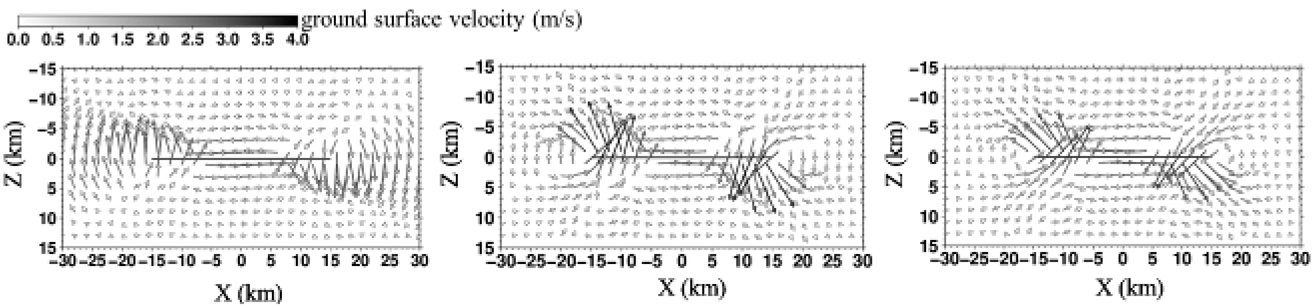


(a) Case 1 (b) Case 2-3 (c) Case 2-5

Fig.4 The maximum ground velocity vectors on the surface

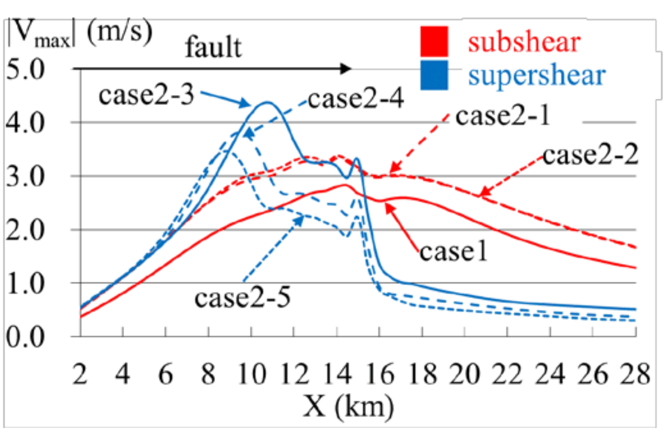


Fig.5 The maximum fault-normal velocity along the surface fault

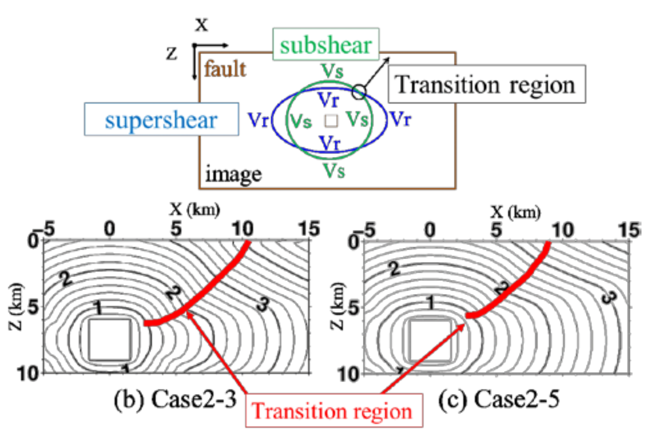


Contour plot of rupture front

Fig. 6 Spread way image view of rupture in the fault and transition region of $V_r$ and $V_s$

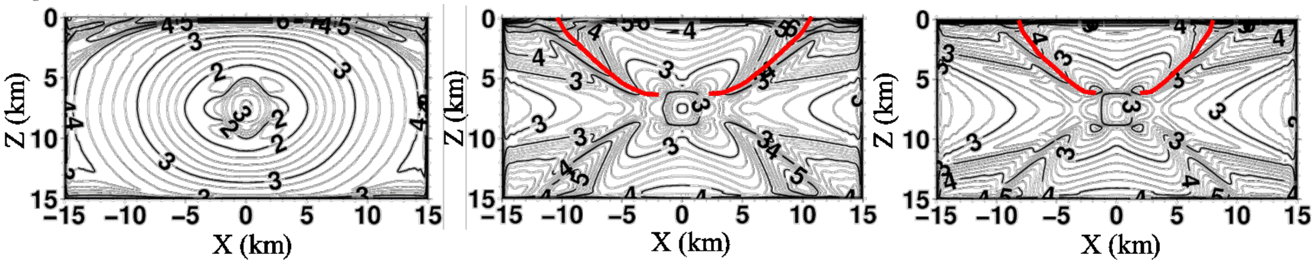


(a) Case 1 (b) Case 2-3 (c) Case 2-5

Fig.7 The maximum slip velocity on the fault (Red line is transition region)

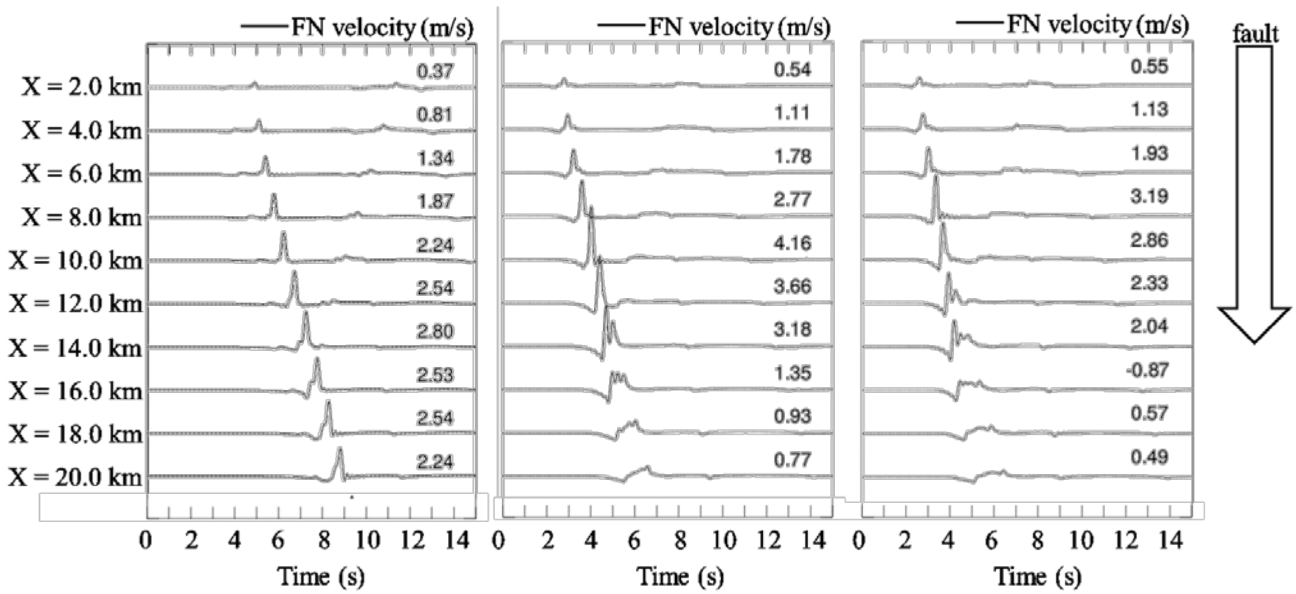


(a) Case 1 (b) Case 2-3 (c) Case 2-5

Fig. 8 Velocity waveforms along the fault on the ground surface (|$V_{max}$| is shown for each waveform)

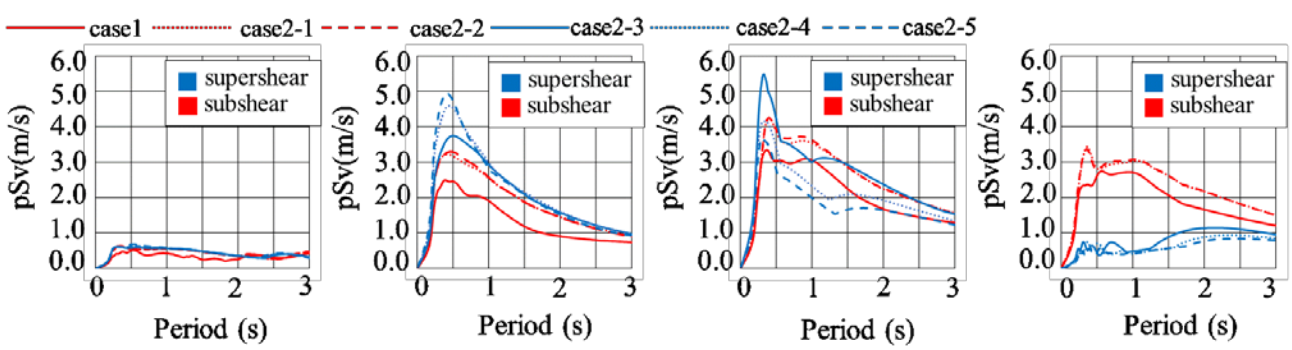


$X$ = 2.0 km $X$ = 8.0 km $X$ = 14.0 km $X$ = 20.0 km

(a) Near epicenter (b) Behind fault tip (c) Near fault tip (d) Ahead of fault tip

Fig. 9 Pseudo-velocity response spectra ($h$ = 5%) along the fault on the ground surface

# 3. Analysis of large strike-slip earthquakes

## 3.1 Analysis model and parameters for dynamic rupture model

In some of the investigated large strike-slip earthquakes occurred in the world, supershear rupture was inferred from observed ground motions. We have examined the ground motion and rupture propagation characteristics in case of larger fault length than previous cases.

Fig. 10 shows the model used for the present analysis; which is the same as that shown in Fig. 2 except an increased fault length. Table 3 gives the different fault parameters for the four large strike-slip earthquake cases (Cases 3-1 to 3-4). Case3-1 has enlarged fault length of 90 km from Case 1. In Cases 3-2, 3-3, and 3-4, the critical displacement was 0.5405 m, the depth of the initial crack was 3.75 m, and a buried crustal earthquake was considered, respectively. The other initial conditions were the same as in the previous analysis (Table 1). The analysis time was increased to 30 s because of the increased fault length.

## 3.2 Dynamic rupture propagation characteristics of large strike-slip earthquakes

Fig.11 shows contours for the rupture arrival times on the fault. Supershear rupture occurred in Case 3-1 from the ground to obliquely downward from the fault after the rupture reached the ground surface. Kaneko and Lapusta suggested that the cause of this phenomenon is the occurrence of total reflection as a result of the angle exceeding the critical value[6)]. Supershear rupture generated from the ground surface is affected by the critical displacement. In Case 3-2, supershear rupture occurred between the fault center to a distance of 36 km from the fault center, but subshear rupture occurred from 36 km to the fault tip. In Cases 3-3 and 3-4, supershear rupture has not occurred. The reason for this is the change in the interaction between the ground surface and the fault resulting from the change in the critical displacement and depth of the initial crack. Fault rupturing in the vicinity of the initial crack in Case 3-2 is slow, requiring the longest amount of time to arrival at fault tip.

Fig. 12 shows the maximum velocity distributions along the fault on the ground surface. In the FN direction, the magnitude of the maximum velocity in the supershear region for Case 3-1 was small at the fault tip, because the difference between $V_r$ and $V_s$ is large. In contrast, the peak maximum velocities in Cases 3-2 and 3-3 were located at the fault tip. In case $V_r$ is close to $V_s$, as a result of the transition from supershear to subshear rupture, concentration of propagating waves occurred due to the increase in the rupture directivity effect. The position of the peak value of $|V_{max}|$ in Case 3-4 (buried crustal earthquake) was similar to that in Case 3-1.

## 3.3 Strong ground motion in near source region

Fig.13 shows the pSv ($h$ = 5%) along the fault on the ground surface. The present analysis model, which has a fault length of 30 km, tends to yield a higher pSv at a short period of approximately 0.5 s than the previous analysis model with a fault length of 15 km (Fig.9). However, the point where is a distance of more than 15 km from the epicenter along the fault was found to have grown pSv in the period between 1.0 and 2.0 s, which greatly influences the structural responses, as seen in the Kobe cases.

In Case 3-1, the predominant period increased as the supershear rupture approached the fault tip. The shift of the peak to the long period range is partly due to gradual increase of the difference between $V_r$ and $V_s$. This also leads to reduction of pulse-like ground motion amplitude.

The predominant period for Case 3-2 increased as the supershear rupture approached the fault tip. The predominant period was 1.0 s at the fault tip, and the pSv was also large under the influence of the rupture directivity effects. Case 3-3, which has a shallow initial crack, had the largest pSv among the studied cases. The reason for this is the large rupture directivity effects where $V_r$ is almost identical to $V_s$. In Case 3-3, the predominant period remained constant along the fault. Case 3-4 had the smallest pSv among the studied cases due to small slip displacement close to ground surface.

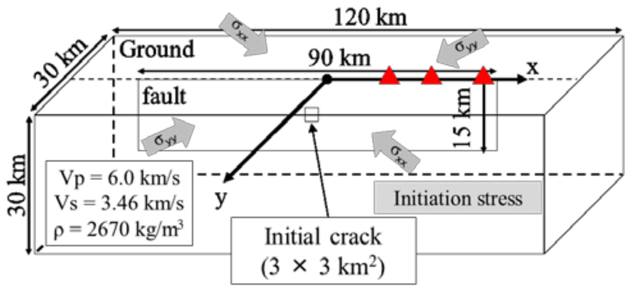


Fig.10 Analysis model

Table 3 Fault parameters for large strike-slip cases

| Case name | case3-1 | case3-2 | case3-3 | case3-4 |
|---|---|---|---|---|
| Clitical displcacement (Dc) | 0.4 m | 0.5405 m | 0.4 m | 0.4 m |
| depth of initial crack | 7.5 km | 7.5 km | 3.75 km | 8.0 km |
| Distance between fault top line and ground | 0 km | 0 km | 0 km | 0.5 km |

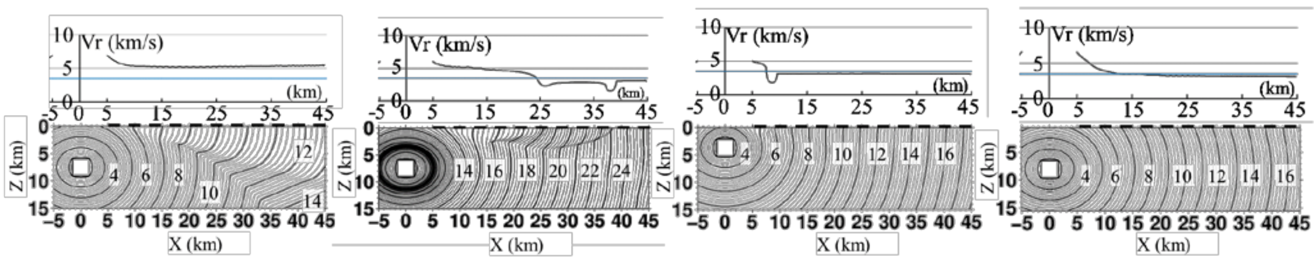


(a) Case 3-1 (b) Case 3-2 (c) Case 3-3 (d) Case 3-4

Fig.11 Contour plots of rupture front and graphs of the rupture velocity on ground surface

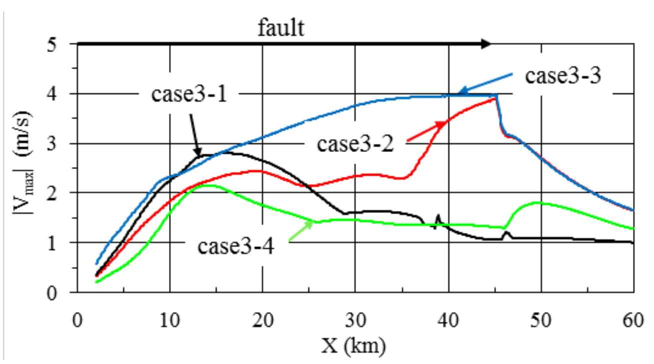


Fig.12 The maximum fault-normal velocity along the surface fault

■ : case3-1 ■ : case3-2 ■ : case3-3 ■ : case3-4 (Broken line: supershear rupture, solid line: subshear rupture)

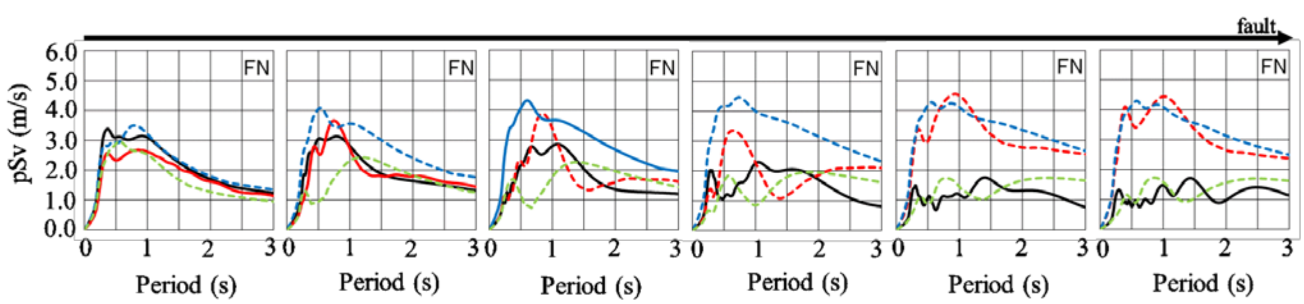


$X$ = 14.0 km $X$ = 22.0 km $X$ = 26.0 km $X$ = 34.0 km $X$ = 42.0 km $X$ = 44.0 km

Fig.13 Pseudo-velocity response spectra ($h$ = 5%) along the fault on the ground surface

# 4. Structural response in near-source region based on dynamic rupture model

## 4.1 Analysis model and considered parameters

The target building in this study is a 30-story reinforced concrete structure, constructed parallel to seismic fault. A three-dimensional moment resisting frame was constructed based on the previously designed analysis model. The base of structure is fixed to the ground. Fig. 14 shows the floor plan and elevation of the building. Columns and beams were modelled by beam elements, which have bending and shearing stiffness. Fig. 15 shows the natural period and modal participation of the building.

The columns were modeled by a multiaxial spring model to include nonlinear effects due to two bending moments and axial force. For the beams, nonlinear rotational springs are used to incorporate nonlinear behavior. Nonlinear dynamic response analyses were done for various types of input motions calculated in the previous sections. The inputs for the earthquake response analysis were the bidirectional ground motions. The momentary stiffness-proportional damping was set to 1.0% for the first natural period.

## 4.2 Building responses for input motions based on dynamic rupture model

The building response is investigated for various pulse-like ground motions based on dynamic rupture model. Firstly, ground motions for supershear and subshear rupture cases in Chapter 2 was used for input motions. Fig. 16 shows the input acceleration waveforms for Cases 1, 2-3, and 2-5 at $X$ = 2.0, 8.0, and 14.0 km. The site of the observation point is indicated by the red triangle in Fig. 2. Fig. 17 shows the heightwise distribution of the maximum interstory drift angle obtained from the response analysis.

In all cases except $X$ = 2.0 km, the interstory drift angles exceed 1/100 rad. where damages were concentrated at lower floors because intense pulse-like motion hits to the lower floor. In Case 1, variation of the interstory drift angles for three sites is small above the 20th floor. Case 2-3 showed the largest response among the considered cases. In this case, the interstory drift angle at the top of the building increased as the site approached the fault tip. The interstory drift angle in Case 2-5 increased as the site changed from $X$ = 2.0 to 8.0 km, as in the other two cases.

In general, a large pulse-like input motion with a short predominant period leads to structural damages in the lower floor in the high-rise RC building and wave transmission to the upper floor is deterred resulting in small interstory drift angle in the middle to upper floor. Fig. 18 shows exaggerated displacement of the high-rise RC building and damage distribution of beams and columns in Case 2-3. Flexural yielding occurred at many beam elements especially in the lower floor due to a large pulse-like input motion with a short predominant period. The heightwise distribution of $X$ = 14.0 km for CASEs 2-3 and 2-5 shows relatively large interstory drift in middle floors, partly because of two pulses generated as a consequence of supershear rupture.

Next, the building response to supershear and subshear rupture cases in Chapter 3 was investigated. Fig. 19 shows the input acceleration waveforms for Cases 3-1, 3-2, and 3-3 at $X$ = 22.0, 34.0, and 44.0 km. The site of the observation point is indicated by the red triangle in Fig. 10.

Fig. 20 shows the heightwise distribution of the maximum interstory drift angle obtained from response analysis. In most cases, responding level was quite large and damage concentration was seen at lower floors, as shown in the previous section.The interstory drift angle in Case 3-1 is smaller than Cases 3-2 and 3-3, where supershear rupture occur in whole fault area and pulse-like ground motion amplitude were reduced.

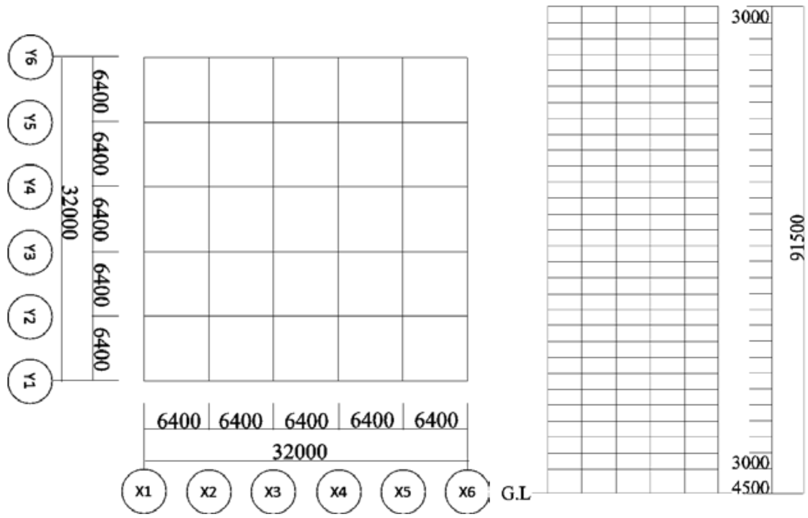


Fig. 14 Floor plan and elevation of target building

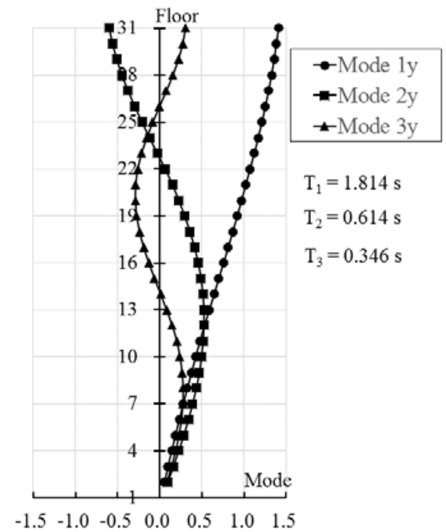


Fig. 15 modal participation

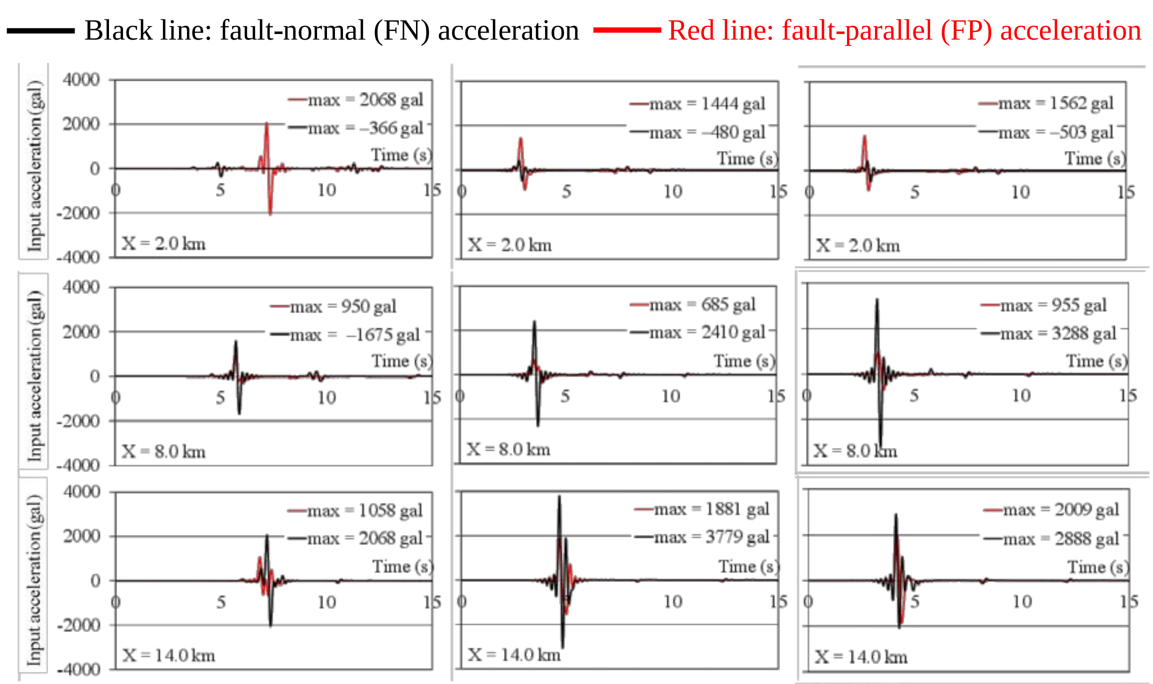


(a) Case 1 (b) Case 2-3 (c) Case 2-5

Fig.16 Input ground acceleration for various cases

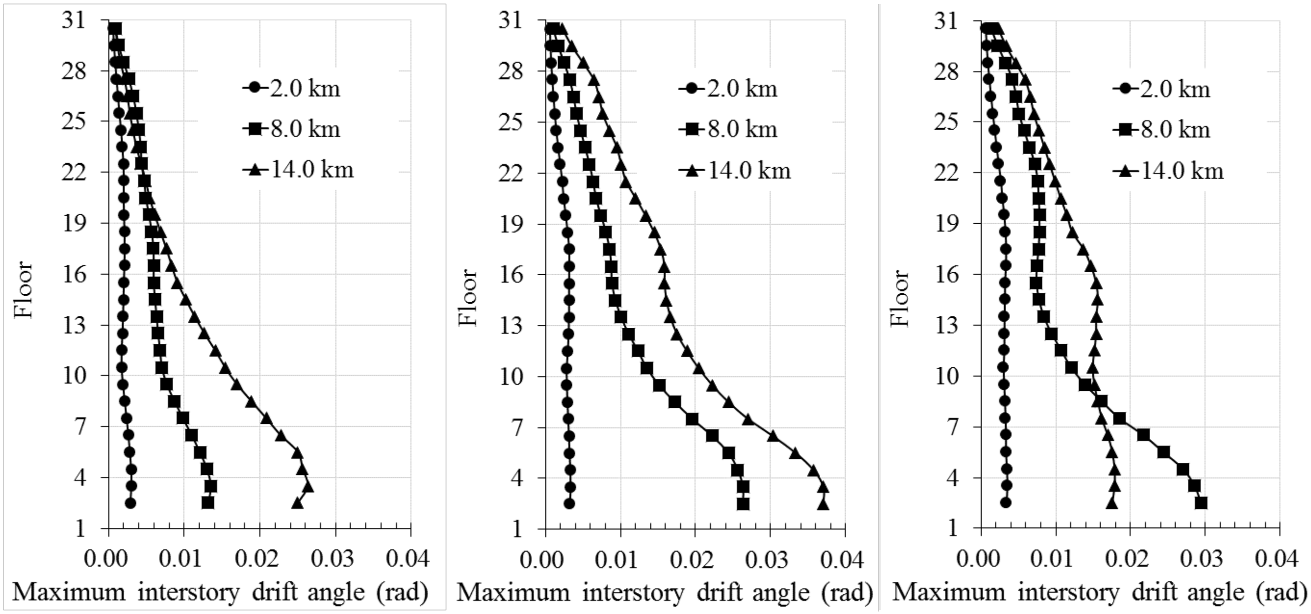


(a) Case 1 (b) Case 2-3 (c) Case 2-5

Fig.17 Heightwise distribution of maximum interstory drift angle obtained from response analysis

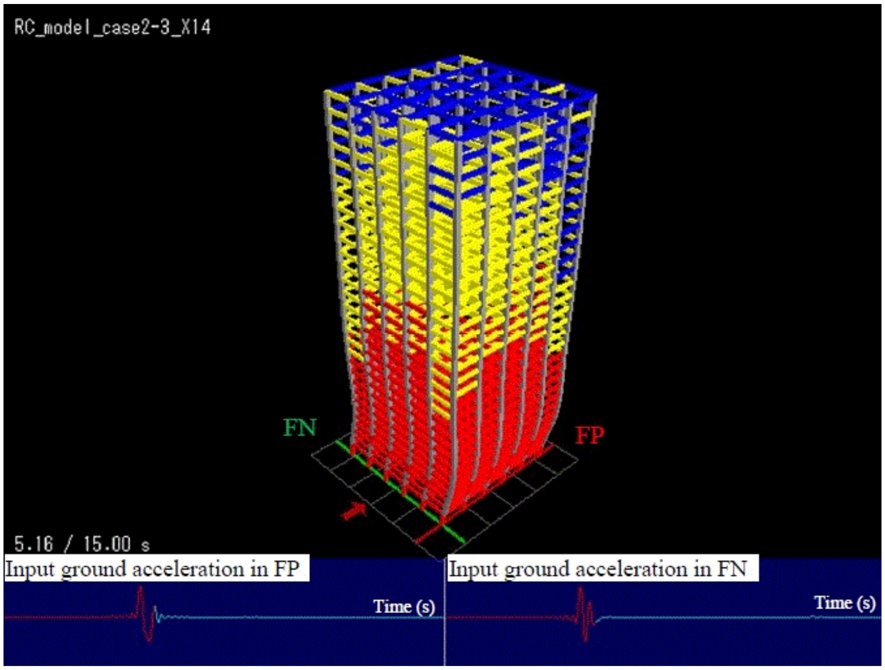


Fig. 18 Exaggerated displacement of the high-rise RC building and damage distribution of beams and columns in Case 2-3

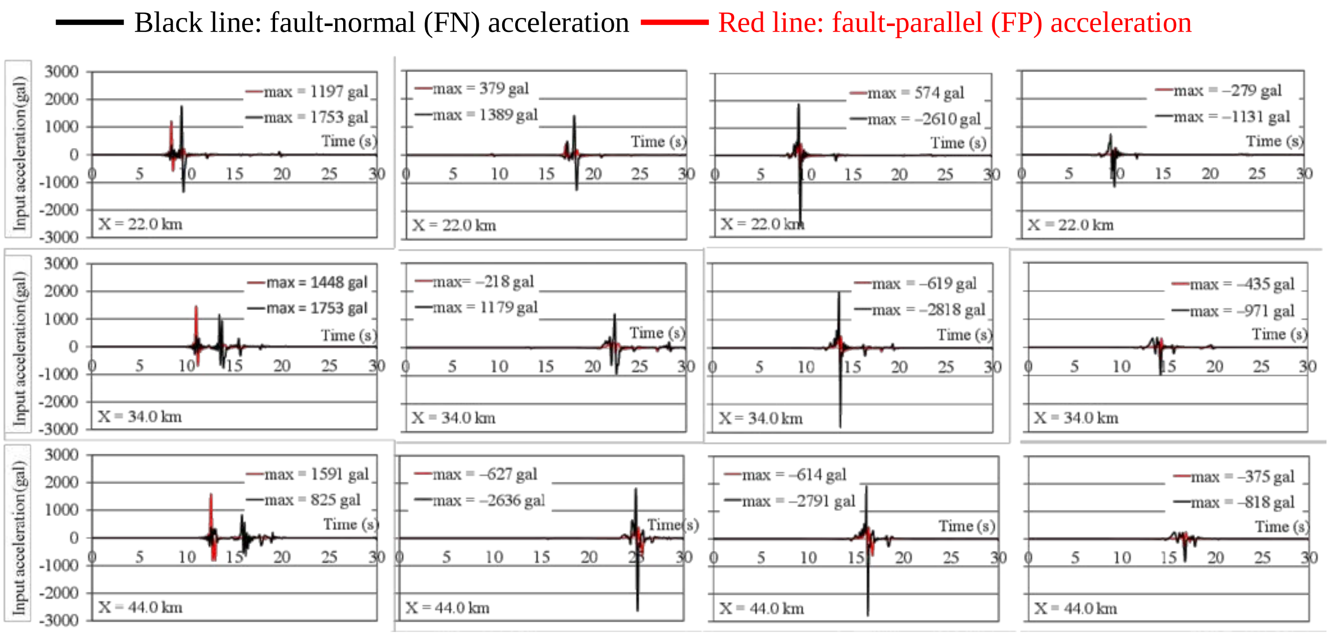


(a) Case 3-1 (b) Case 3-2 (c) Case 3-3 (c) Case 3-4

Fig.19 Input ground acceleration for various cases

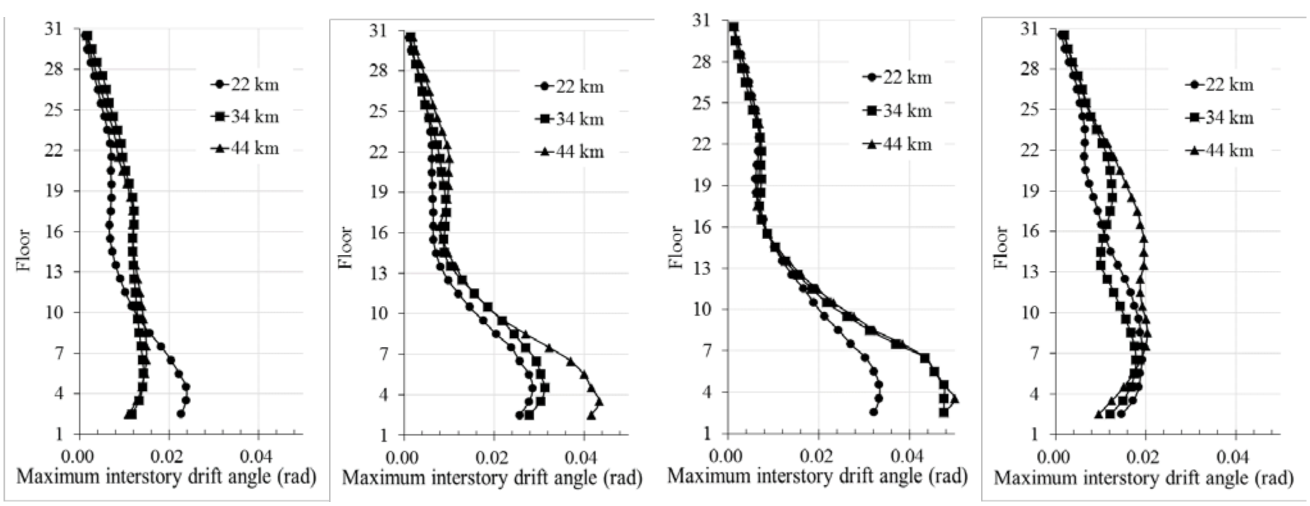


(a) Case 3-1 (b) Case 3-2 (c) Case 3-3 (d) Case 3-4

Fig.20 Heightwise distribution of maximum interstory drift angle obtained from response analysis

## 5. Conclusion

The strong ground motion adjacent to the seismic fault accompanied by supershear and subshear rupture is investigated. A parameter analysis of the weakening friction law, the depth of the initial crack, and the fault length was conducted. The spatial variation of pulse-like ground motions and rupture propagation process of seismic fault were considered in the case of supershear rupture. In addition, the differences in the structural response to seismic waves accompanied by supershear and subshear rupture were discussed for a 30-story reinforced concrete building.

Findings of this study are summarized as follows:

1. The transition region between supershear and subshear rupture was determined through the parameter analysis of the friction law. Ground motions corresponding to the transition region were largely amplified and ground motions with two pulses were seen away from epicenter.

2. In case of large strike-slip earthquakes, supershear rupture occurred from the ground surface to obliquely downward from the fault after the subshear rupture reached the ground surface.

3. From the pseudo-velocity response spectra pSv (h= 5 %) along the fault on the ground surface, the predominant periods in the supershear and subshear cases were shorter than 0.5 s. The shift of the peak to the long period range and reduction of pulse-like ground motion amplitude were seen in the full supershear rupture case for the large strike-slip earthquakes, where the difference between Vr and Vs gradually increased.

4. The seismic responses of a 30 story high-rise RC building to pulse-like motions including supershear rupture cases were studied. In general, a large pulse-like input motion with a short predominant period leads to structural damages in the lower floor in the high-rise building and wave transmission to the upper floor is deterred resulting in small interstory drift angle in the middle to upper floor. The interstory drift angle was relatively small in the case where supershear rupture occur in whole fault area and pulse-like ground motion amplitude were reduced.

## Acknowledgements

We are grateful for comments and suggestions from Dr. Y. Kase (Advanced Industrial Science and Technology) to revise this paper. We used Generic Mapping Tools (GMT 4) by Wessel and Smith[7)] to create contours and other graphs.

## References

1) Y. Kase & K. Kuge: Rupture Propagation beyond Fault Discontinuities: Significance of Fault Strike and Location, Geophys, J. Int, 147, pp330-342, 2001.
2) D. J. Andrews: Rupture Velocity of Plane Strain Shear Cracks, Journal of Geophysical Research, 81, 32, 5679-5687, 1976.
3) H. Yue et al. : Supershear rupture of the 5 January 2013 Craig, Alaska (Mw 7.5) earthquake, Journal of Geophysics Research, 118, 5903-5919, 2013.
4) E. M. Dunham & R. J. Archuleta: Evidence for a supershear Transient during the 2002 Denali Fault Earthquake, Bulletin of the Seismological Society of America, 94, 6B, ppS256- S268, 2004.
5) M. Nagano & K. Kato & R. Ueda & T. Uetake & K. Hikima & H. Ohstuka : Fudamental study on pulsetype earthquake motion near seismic fault based on dynamic rupture model, AIJ J.Technol. Des. Vol. 21, No.47,pp83-88, Feb, 2015
6) Y. Kaneko & N. Lapusta: Supershear transition due to a free surface in 3-D simulations of spontaneous dynamic rupture on vertical strike-slip faults, Tectonophysics, 493, pp272-284, 2010.
7) P. Wessel & W. H. F. Smith: New, improved version of Generic Mapping Tools released, EOS Trans Am Geophys Union. 79, 579, 1998.